1996

Analysis of a Mathematical Model of Mitotic Regulation in Early Oocyte Cells of Xenopus Loevis: The Search for Oscillatory Behavior

Melanie Anderson
The University of Montana
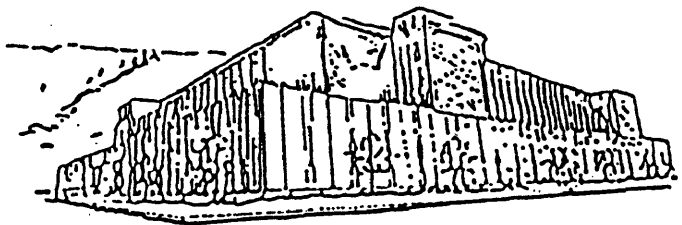
Maureen and Mike

MANSFIELD LIBRARY

The University of **MONTANA**

Permission is granted by the author to reproduce this material in its entirety, provided that this material is used for scholarly purposes and is properly cited in published works and reports.

*** Please check "Yes" or "No" and provide signature ***

Yes, I grant permission   _X_

No, I do not grant permission   _____

Author's Signature _Melanie Anderson_

Date _May 3 1996_

Any copying for commercial purposes or financial gain may be undertaken only with the author's explicit consent.

ANALYSIS OF A MATHEMATICAL MODEL FOR MITOTIC REGULATION IN

EARLY OOCYTE CELLS OF *XENOPUS LAEVIS*:

THE SEARCH FOR OSCILLATORY BEHAVIOR

by

Melanie Anderson

B.S. Gonzaga University, 1993

presented in partial fulfillment of the requirements

for the degree of

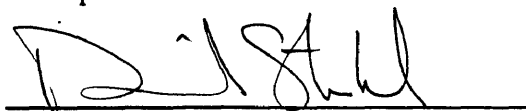Master of Arts

Department of Mathematical Sciences

The University of Montana

1996

Approved by:

_____

Chairperson

_____

Dean, Graduate School

_____

5-3-96

Date

UMI Number: EP72608

UMI®

Dissertation Publishing

UMI EP72608

ProQuest®

Anderson, Melanie, M.A., May 1996　　　　　　　　　　　　　Mathematical Sciences

Analysis of a Mathematical Model for Mitotic Regulation in the Early Oocyte Cells of *Xenopus laevis*: The Search for Oscillatory Behavior (32 pp.)

Advisor: William R. Derrick

   The initiation of mitosis is controlled by a complex called M-phase promoting factor (MPF) made of one subunit each of a protein called cyclin B and a gene product known as cdc2. In the early oocyte stage of frog cells, the MPF system (the MPF dimer together with its enzymes) produces spontaneous cell divisions which are cyclic in time. A previously published paper (Novak and Tyson, 1993a) develops and analyzes a mathematical model which mimics the oscillatory behavior of the frog cells. This model is explored further here; I compare two- and three-dimensional versions and provide evidence for previously undiscovered oscillatory behavior in the form of homoclinic orbits and limit cycles. Recent research provides additional information for the biological process; this paper incorporates the new knowledge and suggests a revised model for analysis.

CONTENTS

LIST OF TABLES

LIST OF FIGURES

v

I. Introduction

Mitosis, the process that cleaves a single mother cell into two identical daughter cells, is one of several cellular activities that have received much research attention in the past two decades. Of particular interest is the reaction that initiates cell division. In the early 1970s, scientists discovered that the concentration of an intracellular protein rose and fell in synchronicity with the cell cycle, peaking immediately prior to each cell division and reaching its lowest levels at the moment of division (Masui and Markert, 1971; Wasserman and Smith, 1978). Calling attention to the protein's cyclic concentration levels, they named it cyclin and surmised its participation in the mechanism (called M-phase promoting factor, or MPF) that initiates cell division (Gerhart *et al.*, 1984; Dunphy *et al.*, 1988; Luca and Ruderman, 1989). Several studies in the 1980s concluded that MPF is actually a dimer (a complex with two parts) made of cyclin and another protein called cdc2 (Dunphy *et al.*, 1988; Labbe *et al.*, 1988). The MPF complex exists in both active and inactive forms; mitosis begins when enough active MPF accumulates inside the cell (Dunphy and Newport, 1988). The interaction of several enzymes activates MPF and will be discussed in detail in this paper. Figure 1 below presents a simplified view of the process.

Many aspects of the MPF reaction seem to be conserved in an evolutionary sense. The
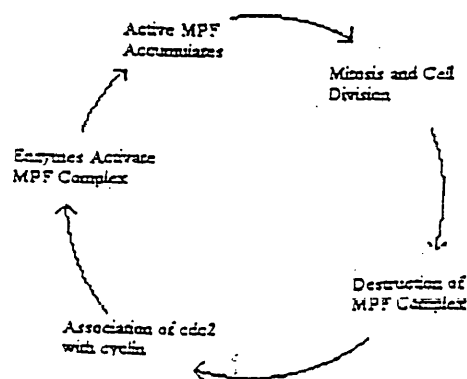

Figure 1: The MPF Cycle

2

structure of the dimer, for example, has been confirmed at least partially for some species of frogs, yeasts, starfish, and sea urchins (Simanis and Nurse, 1986; Dunphy *et al.*, 1988; Labbe *et al.*, 1988; Murray and Kirschner, 1989; Jessus and Beach, 1992). Gould *et al.* (1990) discovered a human homologue to cdc25, one of the enzymes in the reaction. In different species, however, the cell cycle is tied to particular aspects of cell life so that a general model must be adjusted slightly to accommodate these differences. In yeast cells, for example, the initiation of mitosis is tied to DNA replication and cell size, whereas cell division in early frog oocytes proceeds almost entirely without connection to DNA replication and is spontaneously periodic (Wasserman and Smith, 1978).

A more detailed explanation of the cyclin-cdc2 system, with all of its enzymes, is given in the next section. Understanding the MPF reaction becomes quite difficult when we attempt to examine all the details at once; we need to know which parts of the system actually drive the reaction. Approaching this process from a mathematical perspective gives us tools which help determine the vital parts of the system. The goal of a mathematical approach is to build a system of equations whose behavior mimics that of the biological system. In 1993 Novak and Tyson produced, and analyzed several aspects of, a model which replicates the spontaneous oscillations observed in early frog oocytes (Novak and Tyson, 1993a, 1993b). Although their model was not the first (see Goldbetter, 1991; Norel and Agur, 1991; Tyson 1991; Obeyesekere *et al.*, 1992), it was the most comprehensive.

Part II of this paper details the biological information currently known about the MPF reaction. Part III describes the construction of a mathematical model built by Novak and Tyson in 1993 and outlines the method by which the 11 equation system they developed can be reduced down to a two dimensional system. This section also contains an analysis of aspects of the two variable system which Novak and Tyson did not examine. Part IV of this paper examines a three-dimensional mathematical model for the MPF reaction, and compares it to the two variable system. Part V collects the biological data as it pertains to the frog species Xenopus laevis and

presents it in a new system of 11 differential and 4 algebraic equations. Finally, Part VI provides a discussion of this paper's results.

II. The MPF Reaction

The mitotic cell cycle of Xenopus laevis (a species of frog) oocytes has been studied for several decades in an attempt to decipher the mechanism that induces embryonic cells into division. We now know that a complex called M-phase promoting factor (MPF) initiates a string of events which culminates in nuclear and cellular division by phosphorylating histones, lamins, and other substrates (Lewin, 1990; Nurse, 1990). MPF is a dimer composed of two proteins; cyclin B, whose concentration level changes throughout the cell cycle, and cdc2 (Masui and Markert, 1971; Cyert and Kirschner, 1988). At various stages of the cell cycle, the separate pieces of the dimer come together, cleave apart, or are modified by enzymatic activity (see Figure 2a). While the cdc2 subunit provides the location for the protein kinase activity of the dimer, cyclin B functions as a targeting facilitator for the site specific phosphorylation of cdc2 (Simanis and Nurse, 1986; Solomon et al., 1990; Meijer et al., 1991). The total level of cdc2 is constant throughout the cell cycle, and therefore it is the synthesis of cyclin B which drives the early embryonic cycle (Simanis and Nurse, 1986; Gould and Nurse, 1989; Murray and Kirschner, 1989).

Cyclin exists in at least two forms, the more prominent of which are called A and B. They appear to serve different purposes during the cell cycle. Cyclin B is the more active of the two and is vital to the M-phase of the cell cycle. Thus, we will only consider the action of cyclin B, and for notational simplicity we will omit the "B". A second clarification is that MPF is actually defined as that which induces M-phase, or mitosis. In truth mitosis can be initiated by many different processes, of which the cyclin-cdc2 dimer is only one. Therefore, as Novak and Tyson note (1993a), claiming that MPF is the same as the cyclin-cdc2 dimer is erroneous.

(A) MPF DIMER

(B) FEEDBACK LOOPS

KEY

- $\boxed{YT}$ — cdc2
- ○ . cyclin.
- ⊕ phosphate
- AA amino acids.
- UbE Ubiquitin enzyme
- ✳ inactive
- + positive influence

(C) CYCLIN DESTRUCTION
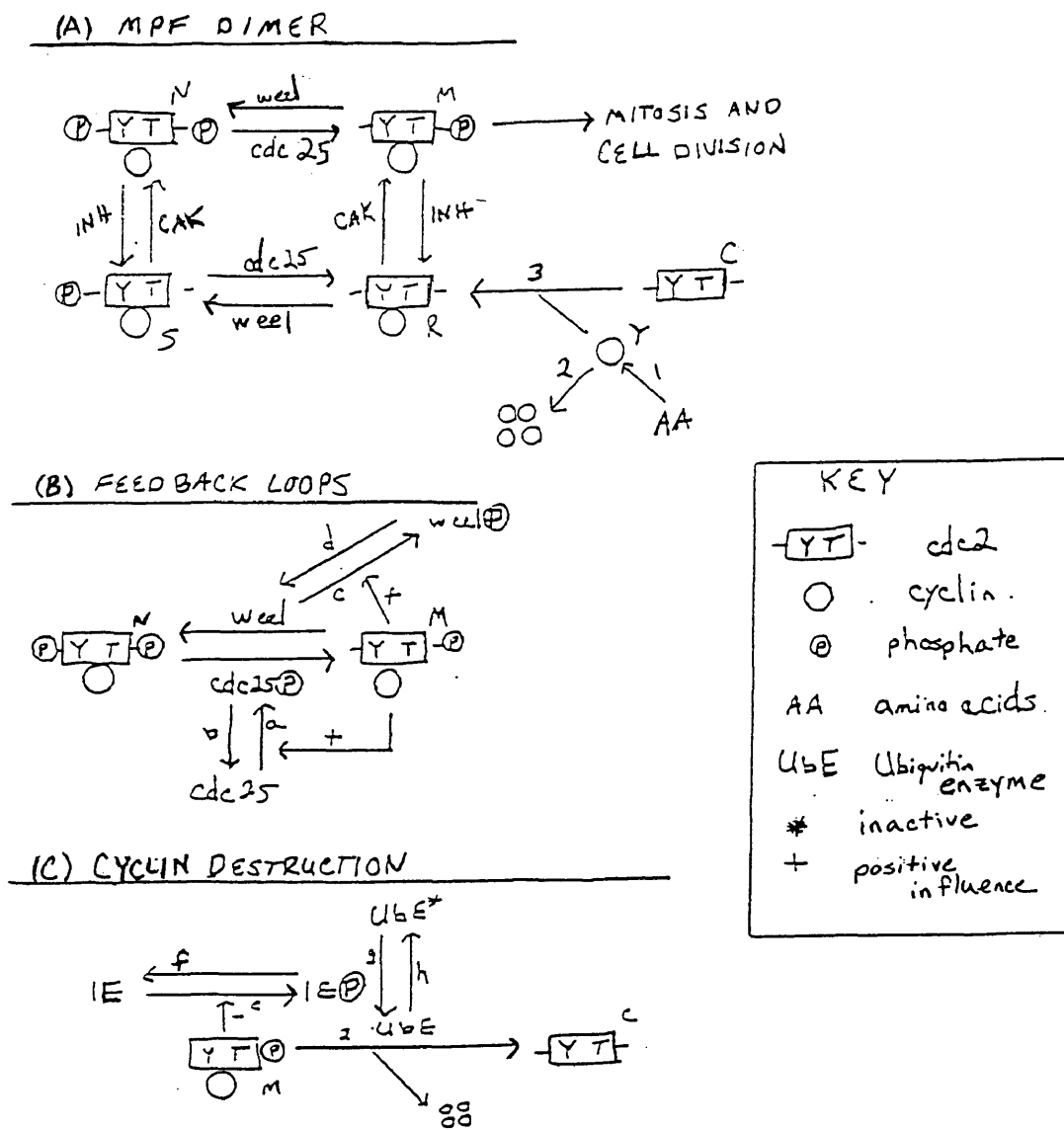
Figure 2. The cdc2-cyclin Mitotic Regulator. This figure depicts all current biological data as pertaining to the early oocyte stage of Xenopus laevis. Arrows indicate direction of enzyme activity; labels correspond to rate constant terms in the equations of section V. A). MPF complex with the activating and inhibiting enzymes; B) Feedback loops; C) Destruction of the MPF dimer through the ubiquitin pathway. Species M in this diagram is the only active from of MPF; species N is "pre-MPF".

Upon noting the distinction, however, we will use "MPF" to mean the dimer for the sake of convenience.

The activity level of MPF is determined by phosphorylation of the cdc2 subunit, which occurs at two sites; threonine-167 (thr-167) and tyrosine-15 (tyr-15). In Figure 2 tyr-15, denoted by Y, is on the left of the cdc2 box and thr-167, denoted by T, is on the right. Phosphorylation at thr-167 is activatory, while phosphorylation at tyr-15 is inhibitory (Gould and Nurse, 1989; Solomon *et al.*, 1990; Gould *et al.*, 1991; Krek and Nigg, 1991; Simanis and Nurse, 1986). Two separate sets of enzymes control the modification of each site. Phosphorylation at thr-167 is controlled by CAK (Cdk activating kinase), which facilitates the reaction, and INH, a type 2A protein phosphatase, which inhibits it (Cyert and Kirschner, 1988; Felix *et al.*, 1990a; Kinoshita *et al.*, 1990; Lee *et al.*, 1991). The modification at the thr-167 site happens at a very rapid rate which does not seem to be regulated during the cell cycle (Gould *et al.*, 1991). Phosphorylation at tyr-15 is controlled by wee1, a tyrosine kinase, and cdc25, a phosphatase (Featherstone and Russell, 1991; Russell and Nurse, 1986, 1987; Gould *et al.*, 1990; Dunphy and Kumagai, 1991; Gautier *et al.*, 1991; Millar *et al.*, 1991; Jessus and Beach, 1992). We also know that MPF activation is an autocatalytic process. There are two positive feedback loops: one through the activation of cdc25 and one through the inhibition of wee1. Active MPF phosphorylates both enzymes, which makes cdc25 more effective at activating MPF and wee1 less effective at inhibiting MPF, as shown in Figure 2b (Cyert and Kirschner, 1988; Kumagai and Dunphy, 1991; Smythe and Newport, 1992; Gerhart *et al.*, 1984; Murray, 1993). Since cdc25 and wee1 oppose each other, the feedback controls ensure that mitotic initiation is irreversible. Two other loops might exist, one through activation of CAK and one through inhibition of INH, but at present there is no evidence for these .

In both frog and yeast cells the MPF dimer accumulates in its inactive forms, primarily in the doubly phosphorylated version called pre-MPF (Devault *et al.*, 1992). Immediately prior to mitosis, the accumulated doubly phosphorylated dimers are then dephosphorylated at tyr-15 (Gould and Nurse, 1989; Gould *et al.*, 1990). To complete mitosis and move on to cell division,

Table 1. Biological and Mathematical Abbreviations

Abbreviation	Description
cdc2	gene product
thr-167	threonine 167; specifies a location on a unit of cdc2
tyr-15	tyrosine 15; another location on a unit of cdc2
INH	an essentially unidentified phosphatase
CAK	Cdk activating kinase
Cdk	Cyclin dependent kinase
wee1	specific tyrosine kinase
cdc25	specific phosphatase
Ube	ubiquitinating enzyme
AA	amino acid
M, N, R, S	specify different species of the MPF dimer
Y	cyclin B monomer
C	cdc2 monomer
k_i	mass action rate constant for step i in the figures
K_i	Michaelis-Mentens rate constant for step i
P	phosphate
T	as a subscript, represents total
IE	intermediate enzyme on the ubiquitin pathway
Y	tyrosine when inside the cdc2 box in figures 2 and 3.1
T	threonine when inside the cdc2 box in figures 2 and 3.1

MPF must be destroyed. Destruction requires the proteolytic cleavage of the cyclin subunit, and MPF prompts this cleavage (Murray *et al.*, 1989; Felix *et al.*, 1990b). The actual proteolysis occurs indirectly, through the ubiquitin pathway as shown in Figure 2c (Felix *et al.*, 1990b; Glotzer *et al.*, 1991). Active MPF stimulates an intermediate enzyme which catalyzes the ubiquitin pathway's degradation of cyclin (Hunt, 1991; Hershko, 1988). This intermediate enzyme is thought to somehow label the cyclin subunits, making it possible for the ubiquitin pathway to detect them. The newly liberated cdc2 subunits are then dephosphorylated so fast that any existing intermediates are undetectable (Luca and Ruderman, 1989; Lorca *et al.*, 1992).

There are alternate cdc2 phosphorylation sites at thr-161 and tyr-14 which may function as part of a backup system. These sites, however, are dominated by thr-167 and tyr-15

respectively and therefore will not be included in our discussion (Lorca *et al.*, 1992). A second tyrosine kinase (mik1) and a second tyrosine phosphatase (Pyp3) have also been found, but since the only known role for mik1 is related to the influence of unreplicated DNA (which is not a factor in Xenopus egg extracts and oocytes) and Pyp3 has been found only in yeast cells, they will not be included either (Lundgren *et al.*, 1991; Millar *et al.*, 1992). Finally, there is evidence for subcellular compartmentalization of the reactions between MPF and its kinases and phosphatases (Alfa *et al.*, 1991; Booher *et al.*, 1989), but at present so little is known about the transport of MPF and the enzymes involved that attempting to include it would be premature.

Several additional discoveries have been made by studying fission yeast cell cycles. Most of these advances have no known homologues in the cellular behavior of frog oocytes, and they are not included in either of the mathematical models we will examine. The consequences of these advances, however, may still provide us with insight, so I have included them here. In fission yeast, the effects of cdc25 and wee1 reveal themselves as changes in cell length at division. Excess wee1 translates into increased cell size, while excess cdc25 expresses itself as decreased cell size (Russell and Nurse, 1986, 1987). Cell size and the enzyme wee1 are related through nim1. The kinase nim1 phosphorylates wee1 on sites which are different from those wee1 uses in its activity with MPF: wee1 phosphorylated in this manner is approximately 25 times less effective in inhibiting mitosis (Enoch and Nurse, 1990; Coleman *et al.*, 1993; Parker *et al.*, 1993; Tang *et al.*, 1993; Wu and Russell, 1993). In other words, nim1 induces mitosis by inhibiting wee1. On the other hand, the yeast cell cycle can be stopped if the DNA is not completely replicated. Unreplicated DNA activates phosphatases that shift cdc25 to its less active, dephosphorylated form, and wee1 to its more active, dephosphorylated form. The net result here is that MPF is rapidly phosphorylated at tyr-15, and is thus inactivated (Smythe and Newport, 1992).

III. Development of a Mathematical Model

In a 1993 paper Novak and Tyson (1993a) collected the information outlined in Sections I and II into a system of 11 differential and 4 algebraic equations, reproduced in Figure 3.2. In developing these equations, Novak and Tyson assumed that mass action kinetics were reasonable in all but two of the reactions. For the reactions describing the activation of cdc25 and UbE the authors used Michaelis-Menten kinetics instead. Mass action kinetics are appropriate for reactions in which the amount of each reactant is very high, so that encounters or collisions occur randomly. Thus, an increase in the amount of reactants would always translate into an increase in the reaction itself. The processes that activate cdc25 and UbE, however, are self limiting in that at some point in the mitotic cycle, an increase of either enzyme forces the cell to divide, which indirectly destroys the enzymes and the reaction stops. This self limiting, or saturation, behavior can be modelled in several ways; Michaelis-Menten kinetics is the preferred method in microbiological and chemical problems (Edelstein-Keshet, 1988). The resulting unwieldy system reduces down to a two variable model under the following assumptions:

(i) the cdc2 subunits liberated after cyclin proteolysis are rapidly dephosphorylated. This assumption has since been substantiated by Lorca *et al.* (1992).

(ii) the exact functions for $k_2(u)$ and $k_{25}(u)$ can be accurately approximated by quadratic functions in u. This assumption is actually based upon another, namely that the activation of UbE and cdc25 occurs rapidly and exhibits "switch-like" behavior.

(iii) MPF dimers phosphorylated at thr-167 are always close to equilibrium. This means that $k_{CAK}[S] \approx k_{INH}[N]$ and $k_{CAK}[R] \approx k_{INH}[M]$.

(iv) cyclin and cdc2 subunits associate rapidly so that the level of free cyclin (species Y) is so low that we can ignore it.

A) The MPF Complex
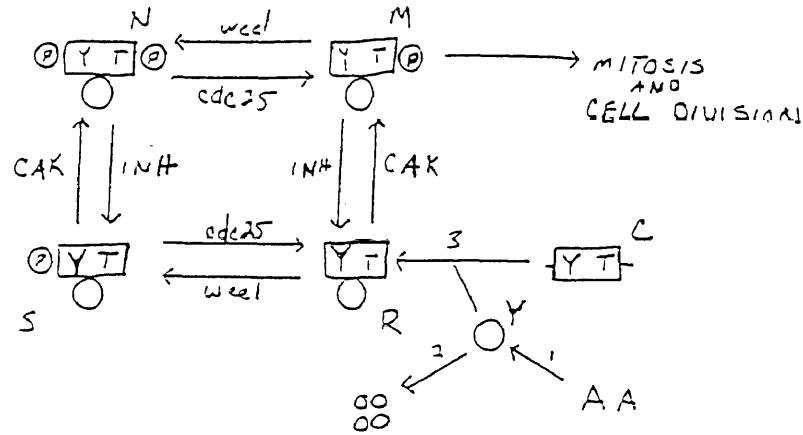
B) FEEDBACK LOOP
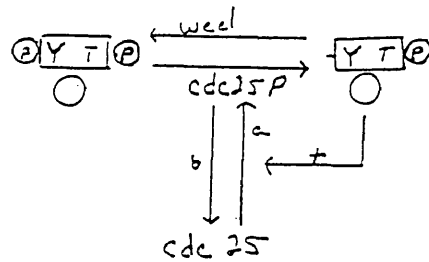
C) CYCLIN DEGRADATION
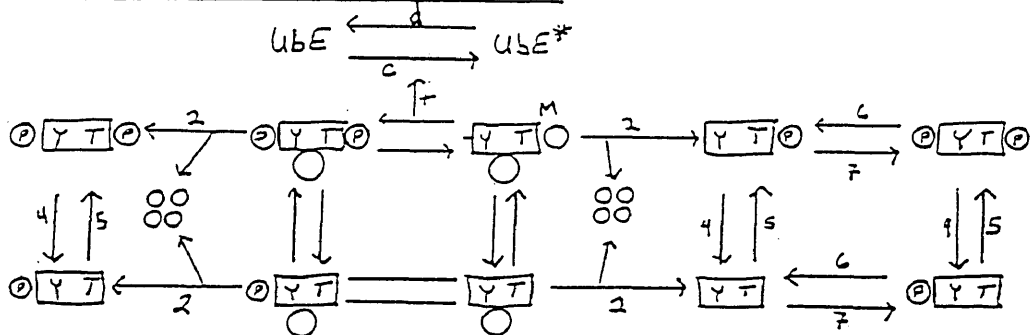
Figure 3.1. Novak and Tyson's 1993 Model. There are several differences between this model and the model in Figure 2, occurring in parts B and C. A). The MPF complex with its accompanying enzymes. B). The feedback loops. Notice that the loop inhibiting wee1 is missing; its existence was not discovered until after publication of the Novak/Tyson model. C). Cyclin Degradation and the Destruction of the MPF Dimer. Much more is now known about this part of the reaction than in 1993, thus there are several differences between this figure and Figure 2c.

Figure 3.2. Novak and Tyson's System of Equations

$$\frac{dY}{dt} = k_1(AA) - k_2Y - k_3YC \tag{3.1}$$

$$\frac{dR}{dt} = -k_2R + k_3YC - k_{CAK}R + k_{INH}M - k_{wee}R + k_{25}S \tag{3.2}$$

$$\frac{dS}{dt} = -S(k_2 + k_{CAK} + k_{25}) + k_{INH}N + k_{wee}R \tag{3.3}$$

$$\frac{dM}{dt} = -M(k_2 + k_{INH} + k_{wee}) + k_{CAK}R + k_{25}N \tag{3.4}$$

$$\frac{dN}{dt} = -N(k_2 + k_{INH} + k_{25}) + k_{CAK}S + k_{wee}M \tag{3.5}$$

$$\frac{d(CP)}{dt} = k_2M + k_5C + k_6(PCP) - (CP)(k_4 + k_7) \tag{3.6}$$

$$\frac{dC}{dt} = k_2R - k_3YC + k_4(CP) + k_6(PC) - C(k_5 + k_7) \tag{3.7}$$

$$\frac{d(PC)}{dt} = k_2S + k_4(PCP) + k_7C - (PC)(k_5 + k_6) \tag{3.8}$$

$$\frac{d(PCP)}{dt} = k_2N + k_5(PC) + k_7(CP) - (PCP)(k_4 + k_6) \tag{3.9}$$

$$\frac{d(cdc25P)}{dt} = \frac{k_a(cdc25)}{K_a + (cdc25)}M - \frac{k_b(cdc25P)}{K_b + (cdc25P)}(INH) \tag{3.10}$$

$$\frac{d(UbE^*)}{dt} = \frac{k_c(UbE)}{K_c + (UbE)}M - \frac{k_d(UbE^*)}{K_d + (UbE^*)} \tag{3.11}$$

with

$$k_{25} = V_{25}'(cdc25) + V_{25}''(cdc25P) \tag{3.12}$$

$$k_2 = V_2'(UbE) + V_2''(UbE^*) \tag{3.13}$$

$$(cdc25) + (cdc25P) = cdc25_{TOTAL} = cdc25_T \tag{3.14}$$

$$(UbE) + (UbE^*) = UbE_{TOTAL} = UbE_T \tag{3.15}$$

The first assumption allowed Novak and Tyson to ignore equations 3.6, 3.8, and 3.9, since species CP, PC, and PCP are thus assumed to have constant, near zero concentrations. By

introducing new variables e = Ube*/Ube$_{Total}$ and u = M/(R+S+M+N+C) the authors

nondimensionalized 3.11, which gives

$$\frac{de}{dt} = \frac{k_c'u(1-e)}{K_c'+1-e} - \frac{k_d'e}{K_d'+e} \qquad (3.16)$$

Setting 3.16 equal to 0 gives the steady state value for e(t). Novak and Tyson then plot e(t) and

an appropriate quadratic function

$$k_2*(u) = k_2' + k_2''(u^2) \qquad (3.17)$$

on the same set of axes, showing that, for $0 \le u \le 0.2$, the actual function 3.13 can be

approximated by the simple quadratic 3.17. The same trick is then applied to 3.10, 3.12, and

3.14. These approximations are justified by assumption (ii) and they cut the number of

differential equations down to six. Due to the fact that total cdc2 concentration in the cell is

constant, equation 3.7 is simply a linear combination of equations 3.2, 3.3, 3.4, and 3.5 so

we may ignore it as well. This leaves us with differential equations for species Y, R, S, M, and

N. At this point, Novak and Tyson introduce dimensionless variables. These new variables in

conjunction with assumption (iii) reduce the number of remaining differential equations down to

three (Part IV contains an analysis of these three equations). Finally, assumption (iv)

allowed the authors to combine two equations from the three dimensional model into a single

differential equation. The resulting two variable system, which describes the action of active

MPF and total cyclin concentration is given by

$$\frac{du}{dt} = \frac{k_1'}{G} - [k_2(u) + k_{wee}]u + k_{25}(u)(\frac{v}{G} - u) \qquad (3.18)$$

$$\frac{dv}{dt} = k_1' - k_2(u)v \qquad (3.19)$$

where

$$u = \frac{[\text{active MPF}]}{[\text{total cdc2}]} = \frac{[M]}{[R+S+M+N+C]} \qquad (3.20)$$

$$v = \frac{[\text{total cyclin}]}{[\text{total cdc2}]} = \frac{[Y+R+S+M+N]}{[R+S+M+N+C]} \qquad (3.21)$$

$$k_2(u) = k_2' + k_2''(u^2) \tag{3.17}$$

$$k_{25}(u) = k_{25}' + k_{25}''(u^2) \tag{3.22}$$

$$k_1' = k_1 \frac{[AA]}{[R+S+M+N+C]} \tag{3.23}$$

$$G = 1 + \frac{k_{INH}}{k_{CAK}} \tag{3.24}$$

Novak and Tyson then applied phaseplane analysis techniques to determine both the location and stability of the equilibrium points, given certain parameter values. For each point in the (u,v) phaseplane, equations 3.18 and 3.19 describe the direction field under which the u and v coordinates change instantaneously. Any particular solution to the system 3.18 - 3.19 is a curve in the phaseplane, beginning at some given initial condition, whose path is dictated by the direction field.

The places in the phaseplane where the solution path is either vertical or horizontal, called nullclines, are typically easy to find. The intersection points of vertical and horizontal nullclines must be stationary in time and are appropriately called steady states or equilibrium points. If we place u on the horizontal axis and v on the vertical axis, the solution path will be vertical wherever u' = 0 and horizontal wherever v' = 0. For us this yields the following equations:

(the vertical nullcline (u' = 0)): $$\qquad v = \frac{Gu(1 + k_{wee} + k_2(u))}{k_{25}(u)} - \frac{k_1'}{k_{25}(u)} \tag{3.25}$$

(the horizontal nullcline (v' = 0)): $$\qquad v = \frac{k_1'}{k_2(u)} \tag{3.26}$$

Novak and Tyson's analysis of this two-dimensional model focused on phaseplane portraits in which the nullclines of the above system intersected at a single point. Examples are included in Figures 3.3a, 3.3b, and 3.3c. This single steady state is either stable or unstable, depending on minor variations in the parameters. For different parameter values, this system

A

B

C

D
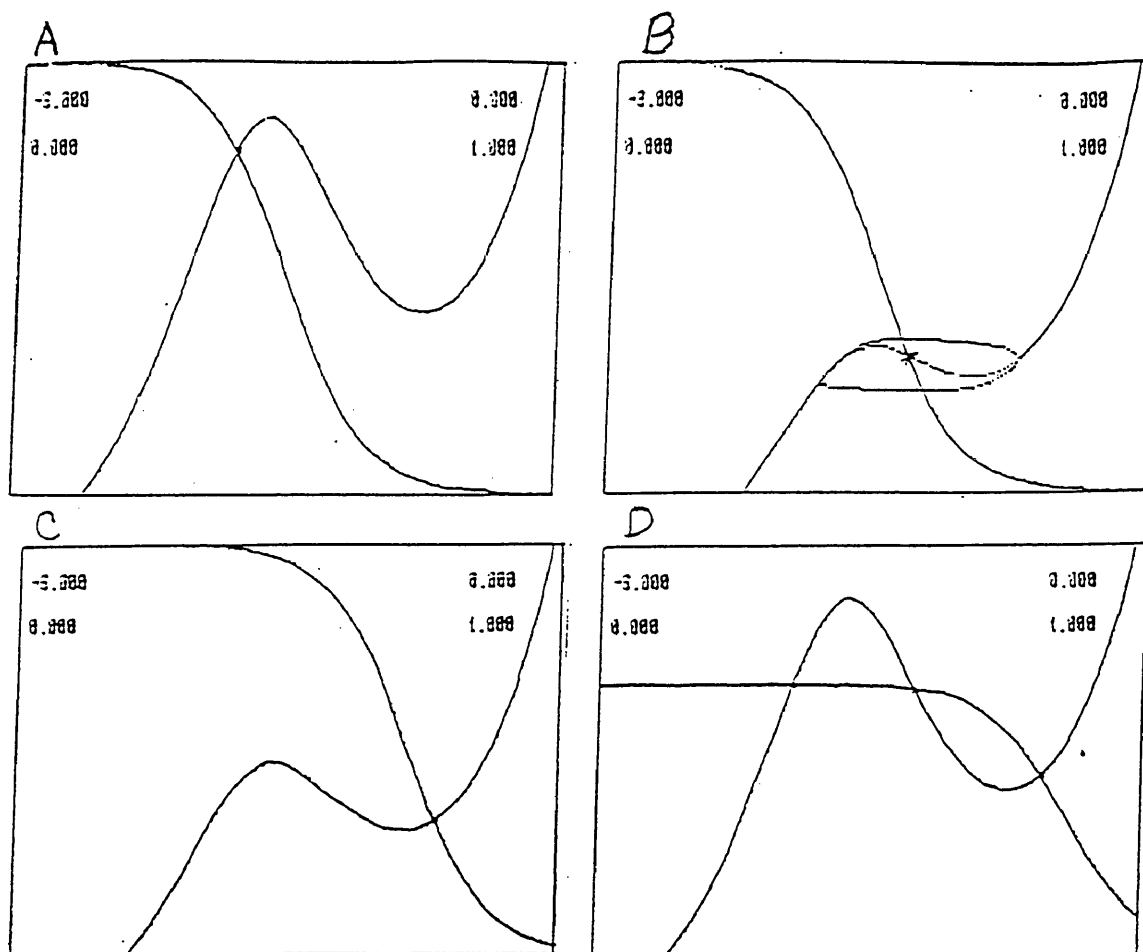
Figure 3.3. Log-linear Phase Portraits. These are plots of the four phase portraits Novak and Tyson presented (1993a). For all portraits, $k_{25}'=.04$, $k_{25}''=100$, $k_1'=.01$. A) A stable node at a low level of active MPF concentration; $k_2'=.01$, $k_2''=10$, $k_{wee}=3.5$. B) An unstable focus; $k_2'=.01$, $k_2''=10$, $k_{wee}=1.5$. The trajectory is a stable limit cycle. C) A stable node at a high concentration of active MPF; $k_2'=.01$, $k_2''=.50$, $k_{wee}=2.0$. D) From left to right; stable node, saddle, stable node. Parameter values are $k_2'=.015$, $k_2''=.10$, $k_{wee}=3.5$.

exhibits two distinct stable equilibrium points. One of these represents a stable state of low MPF activity (see Figure 3.3a), which Novak and Tyson associate with cells arrested in G2, and the other represents a stable state of high MPF activity (Figure 3.3c), which they associate with cells arrested in metaphase. When the equilibrium point is an unstable focus, the system passes

through a Hopf bifurcation, spinning off stable limit cycles which are the oscillations Novak and Tyson were looking for (see Figure 3.3b). The fourth possible interaction of the nullclines, one which simultaneously produces three steady states (Figure 3.3d), was not analyzed. I will concentrate on this situation here.

To produce phase portraits which resemble Novak and Tyson's I substitute $w = \log_{10} u$ and use PhasePlane (Ermentrout, 1988) to plot $w' = 0$ and $v' = 0$. See Figure 3.3 for a list of the parameter values used. The values used in Figure 3.4 all produce portraits with three equilibrium points as in Figures 3.4a and 3.4b. The left most equilibrium point is always stable, though for a small range of parameters it switches from its usual role of a stable node to that of a stable focus. The more central steady state is always a saddle, and therefore has separatrices approaching and leaving the point. On the right is the primary point of interest. For certain parameter values (for this paper I varied k_2'') this point can be an unstable node, unstable focus, stable focus, or stable node. It is the switch from unstable focus to stable focus which is most vital, since this switch indicates the presence of a Hopf bifurcation, which may indicate the initiation or termination of oscillatory behavior. Figure 3.4c is a detail of a trajectory beginning very near the unstable focus. The path winds around and away from the steady state in a tight orbit until it reaches and (due to numerical inaccuracy) crosses the separatrix flowing into the saddle point. The path then quickly moves toward the left most steady state, a stable node.

When the equilibrium point is an unstable focus the separatrices of the saddle may wrap around it to produce a homoclinic orbit, which would also mimic the behavior of the cellular system we are attempting to model. Although I have been unable to determine the homoclinic orbit numerically, Figure 3.5 presents evidence for its existence. Since PhasePlane is a numerical approximation program and is consequently limited in its precision, the separatrix is apparent in forward time only by surrounding it on either side with trajectories as in Figure 3.4d. The direction field shows that orbits beginning just to the right of the separatrix move in toward the unstable focus, while those trajectories beginning just to the left of the separatrix move to the stable node. This fact combined with the oscillations which occur in a small neighborhood of the
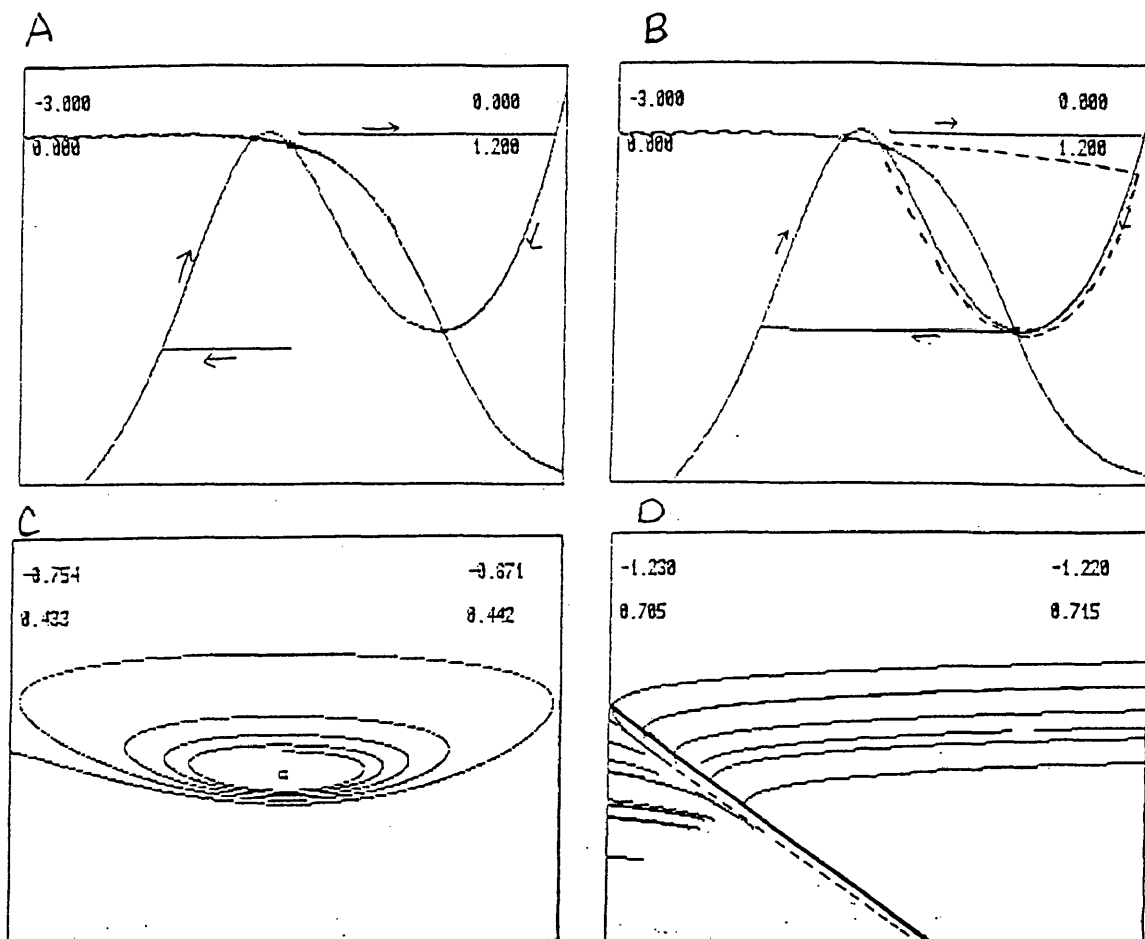
Figure 3.4. The Hopf Bifurcation. Parts (a) and (b) are log-linear plots of the nullclines using w'=0 and v'=0. In (a) the steady states are a stable node, a saddle, and a stable focus, reading from left to right. In (b) they are a stable node, a saddle, and an unstable focus. Each plot includes sample trajectories and arrows indicating the direction of flow. For both (a) and (b) $k_1'=0.01$, $k_{25}'=0.04$, $k_{25}''=100$. Additional parameter values for (a) are $k_2'=0.01$, $k_2''=0.30$, $k_{wee}=4.0$; for (b) the only change is $k_2''=0.40$. The small boxes in (b) outline the areas magnified in (c) and (d). Part (c) depicts the oscillations in a small neighborhood of the unstable focus. The trajectory moving out of the box continues into the stable node in (b). Part (d) is a detail of the trajectories near the separatrix entering the saddle point in (b). In forward time PhasePlane is unable to draw the separatrix directly, but we can get a good idea of its location by examining these near-by paths. The solid line is the nullcline, the dashes represent the approximate location of the separatrix.
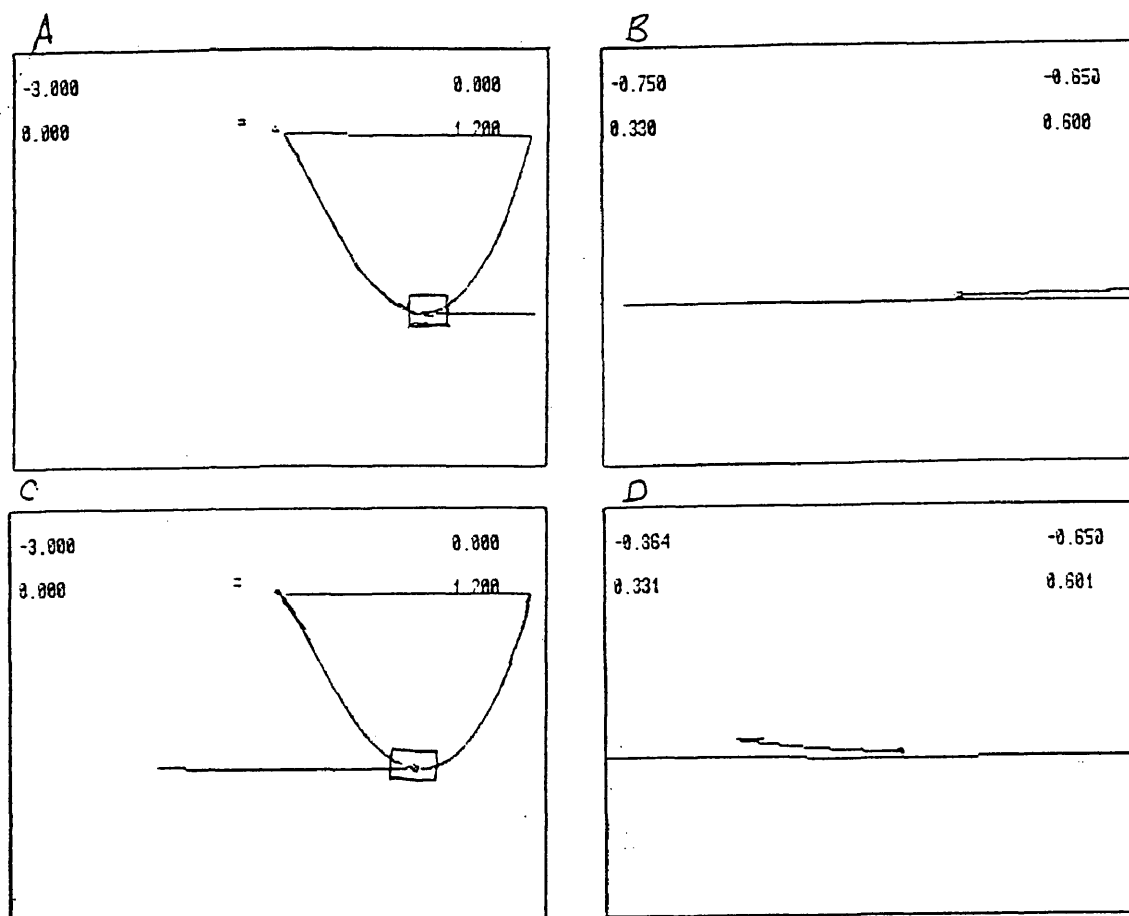
Figure 3.5. Evidence for a Homoclinic Orbit. Parts (a) and (c) are composites of forward and reverse time results (see text for explanation). The steady states in (a) and (c) are as in Figures 3.4a and 3.4c respectively. In (a) the separatrix moving up into the saddle passes just under the equilibrium point, while the trajectory moving into the stable focus from the right meets the point exactly (see part (b)). In (c) the separatrix flowing into the saddle point begins at the unstable focus while the trajectory from the right passes just under the equilibrium point (see (d)). The small boxes within (a) and (c) outline the areas magnified in (b) and (d).

unstable focus provide support for the existence of a homoclinic orbit through the saddle point, along the u' = 0 nullcline, back up the separatrix into the saddle point. Such an orbit (indicated by the dashed trajectory in Figure 3.4b) would provide the model with the periodic oscillations it needs to successfully mimic the cell cycle of Xenopus oocytes.

Finding this path in forward time, however, requires more precision than PhasePlane is capable of. I suspect that as the trajectory winds out of the unstable focus and approaches the

separatrix, the step size (I used dt = .001) causes the trajectory to jump over both the separatrix and the nullcline (since they lie so close together), out of the saddle point's basin of attraction. The trajectory must then travel toward the stable node on the left of the diagram. As a second attempt at locating the separatrix, I substitute s = -t in equations 3.18 and 3.19. Reversing time in this manner switches the stability of all the equilibrium points, so that a path moving from the unstable focus to the saddle point in forward time becomes a path moving from the saddle to the stable focus in reverse time. Figure 3.5 depicts portraits which are composits of the forward and reverse time models. The path from the lower right equilibrium point up to the saddle was obtained using the reverse time model, while the path beginning at the saddle and moving clockwise to the unstable focus was obtained using the forward time model. For Figures 3.5a and 3.5b, I set $k_2'' = 0.30$ which forces the separatrix to pass just under the equilibrium point and the trajectory from the right to exactly meet the steady state. For Figures 3.5c and 3.5d, I set $k_2'' = 0.40$ which forces the two paths to switch positions (compare 3.5b and 3.5d). Therefore, by continuity, there exists some value of k_2'' between 0.30 and 0.40 such that these two paths intersect, creating the homoclinic orbit we seek.

IV. A Three-Dimensional Mathematical Model

While a two dimensional model is relatively easy to analyze and at least partially understand, we run a tremendous risk of losing crucial behavior when we reduce a large system of equations like Novak and Tyson's initial group of 11 down to just two variables. The possibility exists that vital system dynamics are lost when we combine several initial variables into just one. Thus, we should also examine larger models of the same system, looking for dynamics which do not occur in the smaller versions of the problem. Since a system of four or more equations does not allow for graphical representation and is consequently difficult to

understand, I will instead analyze a three-dimensional mathematical model of the cell division regulator.

If we include the level of free cyclin (species Y) by ignoring assumption (iv), the Novak/Tyson three-dimensional model is

$$\frac{dx}{dt} = k_3'(v-x)(1-x) - k_2(u)x \tag{4.1}$$

$$\frac{dy}{dt} = -y[k_2(u) + k_{25}(u)] + k_{wee}(x-y) \tag{4.2}$$

$$\frac{dv}{dt} = k_1' - k_2(u)v \tag{4.3}$$

where

$$k_3' = k_3[\text{total cdc2}] \tag{4.4}$$

$$y = \frac{[S+N]}{[R+S+M+N+C]} \tag{4.5}$$

$$x = \frac{[R+S+M+N]}{[R+S+M+N+C]} \tag{4.6}$$

and $k_2(u)$, $k_{25}(u)$, k_1', and v are given by 3.17, 3.22, 3.23, and 3.21 respectively. As in the two-dimensional model from Section III, v represents the ratio of total cyclin concentration to total cdc2 concentration. The y variable represents the percentage of MPF dimers that are phosphorylated at tyr-15. The final variable, x, represents the proportion of cdc2 that is bound to cyclin.

Notice that if the concentration of unbound cyclin (species Y in Figure 2a) is very small we have

$$v \approx \frac{[R+S+M+N]}{[R+S+M+N+C]} = x \text{ for } 0 \leq v \leq 1 \tag{4.7}$$

This relation is equivalent to assuming the association between free cyclin (Y) and unbound cdc2 (C) happens very fast compared to the other reactions in the system (that is, k_3 is relatively large). If $v > 1$, however, then from 3.21 we must have $Y > C$ and since Y is already assumed small, C must be small as well and thus we define

$$x = \frac{[R+S+M+N]}{[R+S+M+N+C_{small}]} \approx 1 \qquad (4.8)$$

Note that 4.6 forces $x \le 1$. Next, recall from the two dimensional model that

$$u = \frac{M}{[R+S+M+N+C]} \qquad (4.9)$$

Multiplying numerator and denominator by

$$G = 1 + \frac{k_{INH}}{k_{CAK}} = 1.1 \qquad (4.10)$$

yields

$$u = \frac{M(1+\frac{k_{INH}}{k_{CAK}})}{[R+S+M+N+C](1+\frac{k_{INH}}{k_{CAK}})} \qquad (4.11a)$$

which, by assumption (iii), is

$$\approx \frac{[M+R]}{[R+S+M+N+C](1+\frac{k_{INH}}{k_{CAK}})} \qquad (4.11b)$$

$$\approx \frac{[M+R+Y]}{[R+S+M+N+C](1+\frac{k_{INH}}{k_{CAK}})} \qquad (4.11c)$$

$$= \frac{[M+R+Y+S+N-S-N]}{[R+S+M+N+C](1+\frac{k_{INH}}{k_{CAK}})} \qquad (4.11d)$$

$$= \frac{v-y}{1+\dfrac{k_{INH}}{k_{CAK}}} \qquad (4.11e)$$

$$= \frac{v-y}{1.1} \qquad (4.12)$$

We have now defined the relationship between the two and three dimensional variables.

Next, since each variable (x, y, v) represents a ratio of concentrations, we must be sure the model is both well-posed and bounded. If the model is not well-posed then a variable may be negative, while if the model is not bounded, then some variable is growing without limit. Neither situation makes sense biologically; the mathematical model must reflect this reality. For the model to be well-posed, each differential equation must point into the purely positive octant in each of the x - y, y - v, x - v planes. Setting the differentiated variable equal to zero and examining the sign of the resulting equation, we have

$$\frac{dx}{dt}: k_3'v \geq 0 \text{ for } v \geq 0 \qquad (4.13)$$

$$\frac{dy}{dt}: k_{wee}x \geq 0 \text{ for } x \geq 0 \qquad (4.14)$$

$$\frac{dv}{dt}: k_1' > 0 \text{ for all } x, y, v \qquad (4.15)$$

and therefore the trajectories must all stay in the positive octant. Next we discuss boundedness. To begin, we know (from 4.11 and 4.12) that $0 \leq x \leq 1$. Substituting this maximum value for x into 4.2 and 4.3 and setting the results equal to zero yields

$$-y[k_2(u) + k_{25}(u)] + k_{wee}(1 - y) = 0 \qquad (4.16)$$

or

$$y = \frac{k_{wee}}{k_2(u) + k_{25}(u) + k_{wee}} < 1 \text{ since } k_2(u), k_{25}(u) > 0 \qquad (4.17)$$

and $\qquad$ $k_1' - k_2(u)v = 0$ $\qquad$ (4.18)

or $\qquad$ $v = \dfrac{k_1'}{k_2(u)} = \dfrac{.01}{k_2(u)} = \dfrac{.01}{k_2' + k_2''u^2} < 1$ for $k_2' \geq .01$ and $k_2'' > 0$ $\qquad$ (4.19)

Thus the system is both well-posed and bounded; all trajectories must stay inside the first octant with x, y, and v all bounded above by 1.

Next I used PhasePlane to determine the location of the steady states of this three-dimensional model and compared the stability of each point with its analog from the two-dimensional model. Figure 4 places corresponding two-dimensional and three-dimensional plots side-by-side for comparison. Of importance here is the fact that the equilibrium points maintain their stability in the transfer from two- to three-dimensions (see Table 2). Perhaps most importantly, the parameters that produce a stable limit cycle in two dimensions also appear to produce an oscillatory path in three dimensions (Figure 4c: The closed loops in both plots are the limit cycles). Thus the three-dimensional model, for the proper parameter values, also mimics the oscillatory behavior of early frog oocytes. In addition, the three-dimensional model produces several steady states that do not appear in the two-dimensional model. Most of these "extras" do not have biological significance since their coordinates are either negative or out of bounds. These extra steady states do, however, affect the behavior of the trajectories near them and are therefore mathematically significant; they may indicate dynamics which are lost when the model is reduced to just two variables.

Certain values of the parameters produce steady states in the three-dimensional model having two complex eigenvalues whose real parts are positive, and one real eigenvalue that is negative (see Figure 4c and Table 2, line c). This combination of eigenvalues indicates that the system may be chaotic for these parameter values, a result which is not possible in a two-dimensional autonomous system like Novak and Tyson's. Chaos in this problem means that the period between cell divisions is erratic and unpredictable. Thus some cell divisions will happen
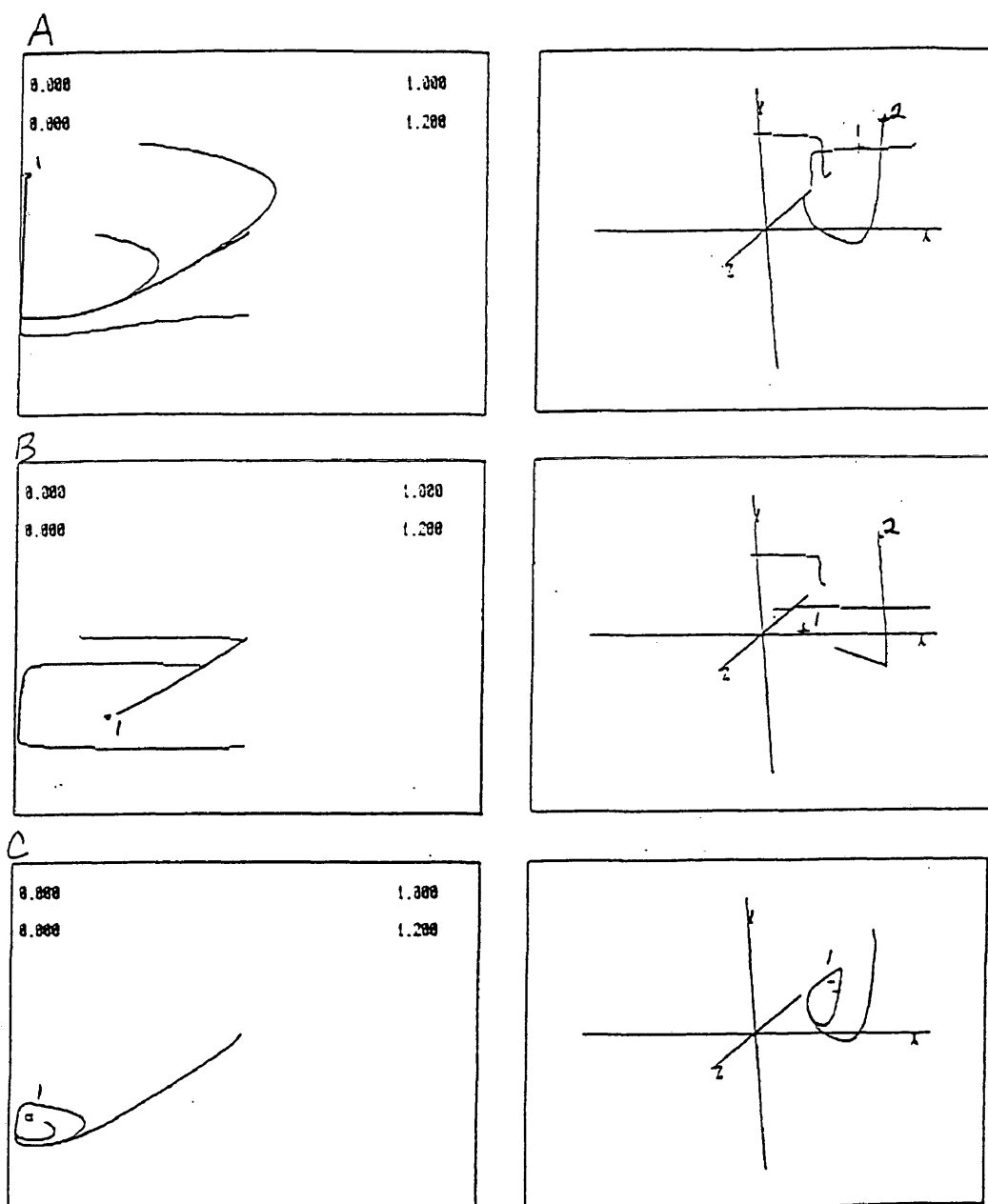
Figure 4. Comparison of Two- and Three-Dimensional Results. Plots of trajectories and steady states for both the two- and three-dimensional versions of the model sit side-by-side, one pair for each set of parameter values. Steady states labeled with the same number exhibit the same behavior. In 4d, for example, the equilibrium point labeled 3 is a stable node in both the two- and three-dimensional cases. Several of the three-dimensional cases produce more steady states than their two-dimensional counterparts. Since these extra steady states influence the behavior of nearby trajectories, they may be indicators of dynamics lost when the mathematical model is reduced to just two variables. Parameter values are as follows: For all cases k_{25}', k_{25}'', k_1' as in Figure 3.3, $k_3'=1000$; A) $k_2'=0.01$, $k_2''=10$, $k_{wee}=3.5$; B) $k_2'=0.01$, $k_2''=0.50$, $k_{wee}=2.0$; C) $k_2'=0.01$, $k_2''=10$, $k_{wee}=1.5$; D) $k_2'=0.015$, $k_2''=0.10$, $k_{wee}=3.5$; E) $k_2'=0.01$, $k_2''=0.3$, $k_{wee}=4.0$; F) $k_2'=0.01$, $k_2''=0.40$, $k_{wee}=4.0$.

Figure 4. Continued

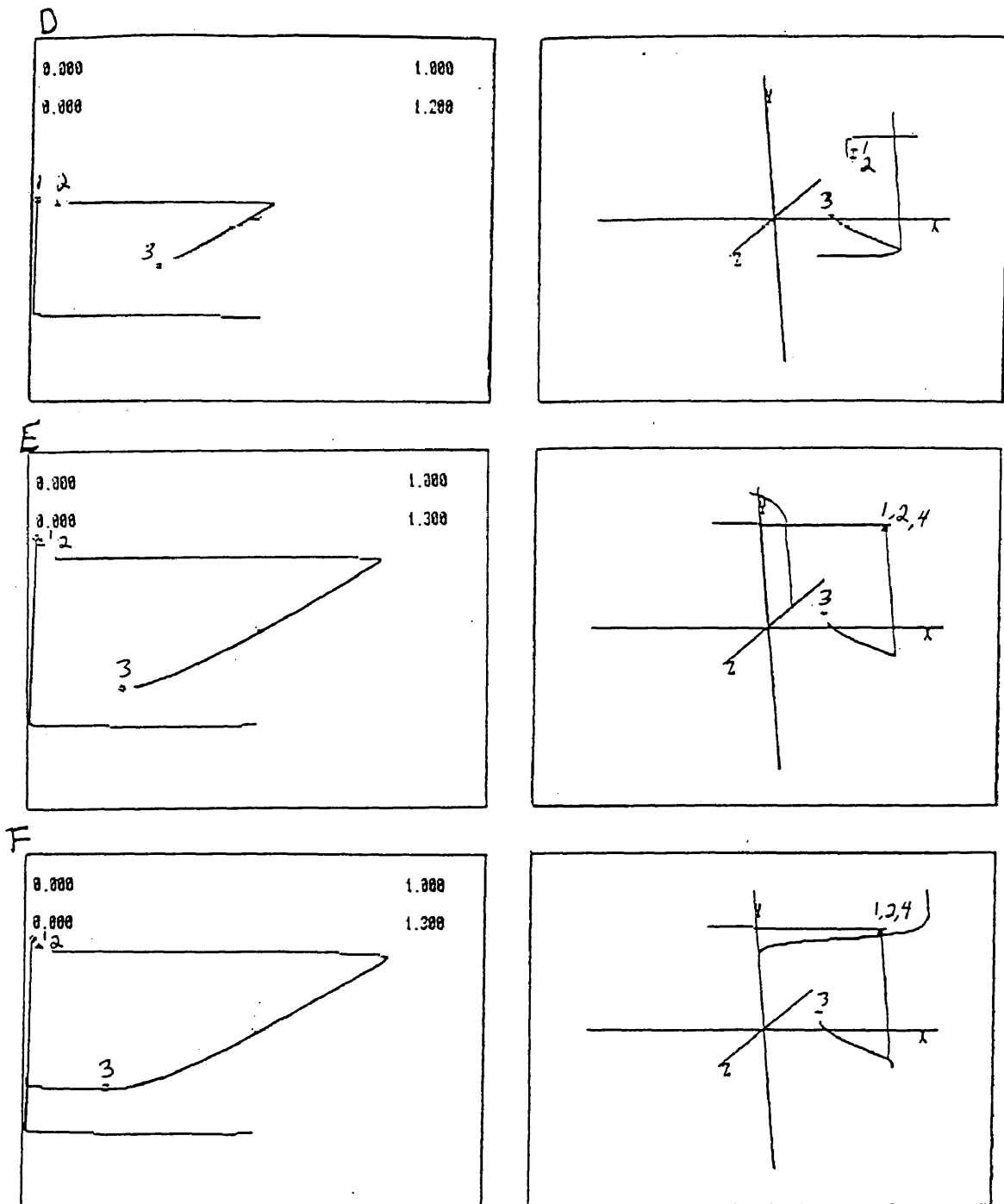too soon (the period is shorter than optimal) and others will happen too late (the period is longer than optimal). Cell cycles outside the optimal time range thus produce daughter cells which are either abnormally small or large. The daughter cells in both cases are unable to support themselves and die. Therefore, for certain parameter values, cell division is lethal, a

Table 2. Steady States of Figure 4: Location and Type

Figure Part	(u, v) coordinates	Type	(x, y, v) coordinates	Type	Comments
a	(.0157, .8016)	r - = 2	(.8005, .7832, .8006)	r - = 3	
			(1.0009, .9865, .9901)	r + = 1, r - = 2	Extra
b	(.2019, .3292)	r - = 2	(.3292, .1071, .3292)	r - = 3	
			(1.0005, .9555, .9786)	r + = 3	Extra
c	(.0463, .3183)	c + = 2	(.3182, .2673, .3182)	c + = 2, r - = 1	
d	(.2761, .4420)	r - = 2	(.4411, .1383, .4420)	r - = 3	
	(.0116, .6661)	r - = 2	(.6660, .6532, .6661)	r - = 3	
	(.0548, .6536)	r + = 1, r - = 1	(.6536, .5934, .6536)	r + = 1, r - = 2	
			(1.0000, .7377, .6177)	r + = 1, r - = 2	Extra
e	(.0189, .9894)	r - = 2	(.9835, .9585, .9841)	r - = 3	
	(.2072, .4372)	c - = 2	(.4372, .2093, .4372)	c - = 2, r - = 1	
	(.0301, .9736)	r + = 1, r - = 1	(.9775, .9477, .9779)	r + = 1, r - = 2	
			(1.0022, .9880, .9977)	r + = 1, r - = 2	Extra
f	(.0197, .9847)	r - = 2	(.9815, .9585, .9820)	r - = 3	
	(.0302, .9648)	r + = 1, r - = 1	(.9649, .9322, .9652)	r + = 1, r - = 2	
	(.1792, .4376)	c + = 2	(.4379, .2409, .4379)	c + = 2, r - = 1	
			(1.0021, .9880, .9972)	r + = 1, r - = 2	Extra

consequence of the mathematical model which may prove to have important medical repercussions.

V. A New Model

Several discoveries have been made since Novak and Tyson published their paper in 1993. These new advances were incorporated into a current model for the MPF reaction in fission yeast (Novak and Tyson, 1995). The yeast model, however, is not directly applicable to Xenopus due to variations in their respective cell cycles. Thus, the Xenopus model in Figure 3.1

needs renovation. There are three major alterations to be made. First, the feedback loop through wee1 was unknown originally and must now be included. Second, we have a better understanding of the destruction of MPF through the ubiquitin pathway. We now know that active MPF stimulates an intermediate enzyme (IE) which then activates the ubiquitin enzyme (UbE), which in turn initiates the proteolysis of cyclin B, turning the cyclin back into amino acids. Finally, we have the fact that the cdc2 subunits released after the cleavage of cyclin B dephosphorylate so fast that intermediates are undetectable.

Figure 2 represents the updated system in three parts: the dimer, the feedback loops, and the ubiquitin action. Using these pictures as a guide, we develop the system of equations in Figure 5. Given the current information about the cell cycle, mass action kinetics are appropriate for most of the steps in the reaction. This aspect of the model may need revision as more knowledge accumulates, but for now mass action constants are considerably easier to work with and the literature does not provide conclusive support for another option. The steps of the reaction which involve the activation of wee1, cdc25, IE and UbE all display saturation behavior and are better modeled with Michaelis-Menten rate terms. We begin the new Xenopus model with a system of 11 differential equations; the task now is to reduce the system down to a number of variables we can analyze concurrently. The following assumptions held for the Xenopus model analyzed in Part III and are still valid:

i) Total cdc2 concentration is constant; total cdc2 = R+S+M+N+C = constant; so
    equation 5.6 is a combination of equations 5.2, 5.3, 5.4, 5.5 and we may ignore it.

ii) The dimers phosphorylated at thr-167 are always near equilibrium so that

$$k_{CAK}S \approx k_{INH}N \text{ and } k_{CAK}R \approx k_{INH}M.$$

These two assumptions, however, leave us with 10 differential equations, nearly all of which are nonlinear. Due to the non-linearities, this new model is quite difficult to reduce further, and I leave the task as an open question.

Figure 5. Equations for New Model

$$\frac{dY}{dt} = k_1(AA) - k_2 Y - k_3 YC \tag{5.1}$$

$$\frac{dR}{dt} = k_{INH} M - (\frac{k_{wee}}{K+R} + k_{CAK} + k_2)R + k_{25}S + k_3 YC \tag{5.2}$$

$$\frac{dS}{dt} = \frac{k_{wee}R}{K+R} - (k_{25} + k_{CAK} + k_2)S + k_{INH}N \tag{5.3}$$

$$\frac{dM}{dt} = k_{CAK}R + k_{25}N - (k_{INH} + k_2 + \frac{k_{wee}}{K+M})M \tag{5.4}$$

$$\frac{dN}{dt} = \frac{k_{wee}M}{K+M} - (k_{INH} + k_{25} + k_2)N + k_{CAK}S \tag{5.5}$$

$$\frac{dC}{dt} = k_2(R + S + M + N) - k_3 YC \tag{5.6}$$

$$\frac{d(cdc25P)}{dt} = \frac{k_a(cdc25_T - cdc25P)}{K_a + (cdc25_T - cdc25P)}M - \frac{k_b(cdc25_T - cdc25P)}{K_b + (cdc25_T - cdc25P)} \tag{5.7}$$

$$\frac{d(wee1)}{dt} = k_d(wee1P) - k_c(wee1)M \tag{5.8}$$

$$\frac{d(wee1P)}{dt} = k_c(wee1)M - k_d(wee1P) \tag{5.9}$$

$$\frac{d(IEP)}{dt} = \frac{k_e(IE_T - IEP)}{K_e + (IE_T - IEP)}M - \frac{k_f(IEP)}{K_f + (IEP)} \tag{5.10}$$

$$\frac{d(UbE)}{dt} = \frac{k_g(UbE_T - UbE)}{K_g + (UbE_T - UbE)}(IEP) - \frac{k_h(UbE)}{K_h + (UbE)} \tag{5.11}$$

with

$$k_2 = V_2'(UbE_T - UbE) + V_2''(UbE) \tag{5.12}$$
$$k_{25} = V_{25}'(cdc25_T - cdc25P) + V_{25}''(cdc25P) \tag{5.13}$$
$$k_{wee} = V_{wee}'(wee1_T - wee1) + V_{wee}''(wee1) \tag{5.14}$$

VI. Discussion

Several criticisms can be leveled at the new model I propose. First, the model does not incorporate the evidence for subcellular localization of the MPF system. As we discover more about the methods cells use to transport the separate pieces of the dimer and the necessary enzymes to the appropriate places, we will need to develop a model that includes this information. For now, however, so little is known about the transport mechanism that including it in the model would require making tremendous and unsubstantiated guesswork. Second, Michaelis-Menten kinetics is only one way to deal with the self-limiting activation of two key enzymes, cdc25 and wee1. The use of some other saturation type rate term might significantly alter the behavior of the mathematical system and could conceivably lead to a more accurate modeling of the biological system.

The mathematical models I have analyzed successfully mimic the behavior of early frog cells by allowing oscillatory trajectories (the limit cycles in Figures 3.3b and 4.1c and the homoclinic orbit in Figure 3.4b). This suggests that the more important parts of the biological reaction are those involving the active form of MPF and cyclin, which we intuitively expect. In the two-dimensional model, these variables are expressed as ratios of concentrations; active MPF and total cyclin to total cdc2. In the three-dimensional model the variables are again expressed as ratios; total cyclin, total tyr-15 inhibited dimers, and total dimers to total cdc2. Thus we have evidence that what drives the mitotic regulator, at least for frog cells, is the relationship between cyclin and potentially active MPF.

A thorough understanding of the cell division cycle may allow us to artificially regulate mitosis in both directions. The ability to inhibit mitosis could potentially give the medical field a new method for treating cancerous tumors. As described in Part IV, inducing chaotic periods between cell divisions may also prove to be beneficial as a treatment option. On the other hand, new treatments for arthritis and cartilage damage in joints use grafts of the patient's own tissue. Currently these grafts take weeks or months to cultivate, whereas the ability to artificially induce

healthy cell division may cut the required growth time down dramatically. Once perfected and available, the ability to rapidly produce grafts may be an effective way to treat burn victims: Skin grafts could be grown, possibly in a matter of hours, using just a few of the victim's surviving cells as starters for the culture, thereby reducing the risk of transplant rejection. For the above reasons, and probably several more, a thorough grasp on the mechanics of mitotic initiation is quite valuable, and mathematical modelling of the process is a vital tool for understanding the biological information.

REFERENCE LIST

Alfa, C. E., Gallagher, I. M. and Hyams, J. S. (1991). Subcellular localization of the p34^{cdc2}/p63^{cdc13} protein kinase in fission yeast. *Cold Spring Harb. Symp. on Quan. Biol.* **56**, 489-494.

Booher, R. N., Alfa, C. E., Hyams, J. S. and Beach, D. H. (1989). The fission yeast cdc2/cdc13/suc1 protein kinase: regulation of catalytic activity and nuclear localization. *Cell* **58**, 485-497.

Coleman, T. R., Tang, Z. and Dunphy, W. G. (1993). Negative regulation of the wee1 protein kinase by direct action of the Nim1/Cdr1 mitotic inducer. *Cell* **72**, 919-929.

Cyert, M. S. and Kirschner, M. W. (1988). Regulation of MPF activity *in vitro*. *Cell* **53**, 185-195.

Devault, A., Fesquet, D., Cavadore, J., Garrigues, A., Labbe, J., Lorca, T., Picard, A., Philippe, M. and Doree, M. (1992). Cyclin A potentiates maturation promoting factor activation in the early Xenopus embryo via inhibition of the tyrosine kinase that phosphorylates cdc2. *J. Cell Biol.* **118**, 1109-1120.

Dunphy, W. G. and Kumagai, A. (1991). The cdc25 protein contains an intrinsic phosphatase activity. *Cell* **67**, 189-196.

Dunphy, W. G. and Newport, J. W. (1988). Mitosis inducing factors are present in a latent form during interphase in the Xenopus embryo. *J. Cell Biol.* **106**, 2047-2056.

Dunphy, W. G., Brizuela, L., Beach, D. and Newport, J. (1988). The Xenopus cdc2 protein is a EdE component of MPF, a cytoplasmic regulator of mitosis. *Cell* **54**, 423-431.

Edelstein-Keshet, L. (1988). *Mathematical Models in Biology*. New York: Random House.

Enoch, T. and Nurse, P. (1990). Mutation of fission yeast cell cycle control genes abolishes dependence of mitosis on DNA replication. *Cell* **60**, 665-673.

Ermentrout, B. (1988). *PhasePlane the Dynamical Systems Tool, Version 2.0*. Pacific Grove, CA: Brooks/Cole.

Featherstone, C. and Russell, P. (1991). Fission yeast p107^{wee1} mitotic inhibitor is a tyrosine/serine kinase. *Nature, Lond.* **349**, 808-811.

Felix, M., Cohen, P. and Karsenti, E. (1990a). Cdc2 H1 kinase is negatively regulated by a type 2A phosphatase in the Xenopus early embryonic cell cycle: evidence from the effects of okadaic acid. *EMBO J.* **9**, 675-683.

Felix, M. A., Labbe, J. C., Doree, M., Hunt, T. and Karsenti, E. (1990b). Triggering of cyclin degradation in interphase extracts of amphibian eggs by cdc2 kinase. *Nature, Lond.* **346**, 379-382.

Gautier, J., Solomon, M. J., Booher, R. N., Bazan, J. F. and Kirschner, M. W. (1991). cdc25 is a specific tyrosine phosphatase that directly activates p34^{cdc2}. *Cell* **67**, 197-211.

Gerhart, J., Wu, M. and Kirschner, M. W. (1984). Cell cycle dynamics of an M-phase-specific cytoplasmic factor in Xenopus laevis oocytes and eggs. *J. Cell Biol.* **98**, 1247-1255.

Glotzer, M., Murray, A. W. and Kirschner, M. W. (1991). Cyclin is degraded by the ubiquitin pathway. *Nature, Lond.* **349**, 132-138.

Goldbetter, A. (1991). A minimal cascade model for the mitotic oscillator involving cyclin and cdc2 kinase. *Proc. Natl. Acad. Sci. USA* **88**, 9107-9111.

Gould, K. L. and Nurse, P. (1989). Tyrosine phosphorylation of the fission yeast cdc2$^+$ protein kinase regulates entry into mitosis. *Nature* **342**, 39-45.

Gould, K. L., Moreno, S., Owen, D. J., Sazer, S. and Nurse, P. (1991). Phosphorylation at thr-167 is required for *Schizosaccharomyces pombe* p34^{cdc2} function. *EMBO J.* **10**, 3297-3309.

Gould, K. L., Moreno, S., Tonks, N. K. and Nurse, P. (1990). Complementation of the mitotic activator, p80^{cdc25}, by a human protein-tyrosine phosphatase. *Science* **250**, 1573-1576.

Hershko, A. (1988). Ubiquitin-mediated protein degradation. *J. Biol. Chem.* **263**, 15237-15240.

Hunt, T. (1991). Destruction's our delight. *Nature* **349**, 100-101.

Jessus, C. and Beach, D. (1992). Oscillation of MPF is accompanied by periodic association between cdc25 and cdc2-cyclin B. *Cell* **68**, 323-332.

Kinoshita, N., Ohkura, H. and Yanagida, M. (1990). Distinct, essential roles of type 1 and 2A protein phosphatases in the control of the fission yeast cell division cycle. *Cell* **63**, 405-415.

Krek, W. and Nigg, E. A. (1989). Differential phosphorylation of vertebrate p34^{cdc2} kinase at the G1/S and G2/M transitions of the cell cycle: identification of major phosphorylation sites. *EMBO J.* **10**, 305-316.

Kumagai, A. and Dunphy, W. G. (1992). Regulation of the cdc25 protein during the cell cycle in Xenopus extracts. *Cell* **70**, 139-151.

Labbe, J. C., Lee, M. G., Nurse, P., Picard, A. and Doree, M. (1988). Activation at M-phase of a protein kinase encoded by a starfish homologue of the cell cycle control gene cdc2$^+$. *Nature* **355**, 251-254.

Lee, T. H., Solomon, M. J., Mumby, M. C. and Kirschner, M. W. (1991). INH, a negative regulator of MPF, is a form of protein phosphatase 2A. *Cell* **64**, 415-423.

Lewin, B. (1990). Driving the cell cycle: M phase kinase, its partners, and substrates. *Cell* **61**, 743-752.

Lorca, T., Labbe, J., Devault, A., Fesquet, D., Capony, J., Cavadore, J., Bouffant, F. and Doree, M. (1992). Dephosphorylation of cdc2 on threonine 161 is required for cdc2 kinase inactivation and normal anaphase. *EMBO J.* **11**, 2381-2390.

Luca, F. C. and Ruderman, J. V. (1989). Control of programmed cyclin degradation in a cell-free system. *J. Cell Biol.* **109**, 1895-1909.

Lundgren, K., Walworth, N., Booher, R., Dembski, M., Kirschner, M. W. and Beach, D. (1991). mik1 and wee1 cooperate in the inhibitory tyrosine phosphorylation of cdc2. *Cell* **64**, 1111-1122.

Masui, Y. and Markert, C. L. (1971). Cytoplasmic control of nuclear behavior during meiotic maturation of frog oocytes. *J. Exp. Zool.* **177**, 129-146.

Meijer, L., Azzi, L. and Wang, J. Y. J. (1991). Cyclin B targets p34^{cdc2} for tyrosine phosphorylation. *EMBO J.* **10**, 1545-1554.

Millar, J. B. A., Lenaers, G. and Russell, P. (1992). Pyp3 PTPase acts as a mitotic inducer in fission yeast. *EMBO J.* **11**, 4933-4941.

Millar, J. B. A., McGowan, C. H., Lenaers, G., Jones, R. and Russell, P. (1991). p80^{cdc25} mitotic inducer is the tyrosine phosphatase that activates p34cdc2 kinase in fission yeast. *EMBO J.* **10**, 4301-4309.

Murray, A. W. and Kirschner, M. W. (1989). Cyclin synthesis drives the early embryonic cell cycle. *Nature, Lond.* **339**, 275-280.

Murray, A. W., Solomon, M. J. and Kirschner, M. W. (1989). The role of cyclin synthesis and degradation in the control of maturation promoting factor activity. *Nature* **339**, 280-286.

Murray, A. W. (1993). Turning on mitosis. *Curr. Biol.* **3**, 291-293.

Norel, R. and Agur, Z. (1991). A model for the adjustment of the mitotic clock by cyclin and MPF level. *Science* **251**, 1076-1078.

Novak, B. and Tyson, J. J. (1993a). Modeling the cell division cycle: M-phase trigger, oscillations, and size control. *J. Theor. Biol.* **165**, 101-134.

Novak, B. and Tyson, J. J. (1993b). Numerical analysis of a comprehensive model of M-phase control in *Xenopus* oocyte extracts and intact embryos. *J. Cell Sci.* **106**, 1153-1168.

Novak, B. and Tyson, J. J. (1995). Quantitative analysis of a molecular model of mitotic control in fission yeast. *J. Theor. Biol.* **173**, 283-305.

Nurse, P. (1990). Universal control mechanism regulating onset of M-phase. *Nature, Lond.* **344**, 503-508.

Obeyesekere, M. N., Tucker, S. L. and Zimmerman, S. O. (1992) Mathematical models for the cellular concentrations of cyclin and MPF. *Biochem. Biophys. Res. Commun.* **184**, 782-789.

Parker, L. L., Walter, S. A., Young, P. G. and Pievnica-Worms, H. (1993). Phosphorylation and inactivation of the mitotic inhibitor Wee1 by the *nim1/cdr1* kinase. *Nature* **363**, 736-738.

Russell, P. and Nurse, P. (1986). cdc25$^+$ functions as an inducer in the mitotic control of fission yeast. *Cell* **45**, 145-153.

Russell, P. and Nurse, P. (1987). Negative regulation of mitosis by wee1$^+$, a gene encoding a protein kinase homolog. *Cell* **49**, 559-567.

Simanis, V. and Nurse, P. (1986). The cell cycle control gene cdc2$^+$ of fission yeast encodes a protein kinase potentially regulated by phosphorylation. *Cell* **45**, 261-268.

Smythe, C. and Newport, J. W. (1992). Coupling of mitosis to the completion of S phase in Xenopus occurs via modulaiton of the tyrosine kinase that phosphorylates p34^{cdc2}. *Cell* **68**, 787-797.

Solomon, M. J., Glotzer, M., Lee, T. H., Philippe, M. and Kirschner, M. W. (1990). Cyclin activation of p34^{cdc2}. *Cell* **63**, 1013-1024.

Tang, Z., Coleman, T. R. and Dunphy, W. G. (1993). Two distinct mechanisms for negative regulation of the Wee1 protein kinase. *EMBO J.* **12**, 3427-3436.

Tyson, J. J. (1991). Modeling the cell division cycle: cdc2 and cyclin interactions. *Proc. Natl. Acad. Sci. USA* **88**, 7328-7332.

Wasserman, W. J. and Smith, L. D. (1978). The cyclic behavior of a cytoplasmic factor controlling nuclear membrane breakdown. *J. Cell Biol.* **78**, R15-R22.

Wu, L. and Russell, P. (1993). Nim1 kinase promotes mitosis by inactivating Wee1 tyrosine kinase. *Nature* **363**, 738-741.